Experiments on tropical circulation with a simple moist model

By M. K. DAVEY and A. E. GILL
Meteorological Office Unit, Hooke Institute for Atmospheric Research, Clarendon Laboratory, Parks Road, Oxford, OX1 3PU

SUMMARY

A simple model of the circulation of the tropical atmosphere is constructed where the circulation is determined entirely by the sea surface temperature (s.s.t.) pattern, or rather by a forcing field which is closely related to s.s.t. It is an equatorial beta-plane model with an assumed simple baroclinic vertical structure. The moisture and precipitation fields are allowed to evolve freely so there are feedbacks between the latent heating, which contributes to driving the motion, and the low-level velocity field which produces the moisture convergence required to generate precipitation.

Experiments with idealized Pacific s.s.t. distributions produce qualitatively realistic precipitation patterns for January (a patch in the west Pacific over the equator) and July (a zonal strip north of the equator).

Analytic solutions for zonally symmetric flow are given to illustrate the basic dynamics and to study the parameter dependence of the precipitation. An analysis of zonal variations shows that a good simplifying approximation for this component is to neglect Rayleigh friction while retaining Newtonian cooling.

The effect of changing the zonal contrast in the prescribed forcing is to gradually alter the circulation from Hadley-like to Walker-like. The model suggests that along the equator a relatively small contrast is needed to break a zonal band of precipitation.

1. INTRODUCTION

Much of the large-scale tropical circulation is directly driven by heat sources and sinks, so considerable insight into the dynamics follows from a study of the response of an atmosphere to sources and sinks placed near the equator. Simple models with fixed heating have been investigated by, for example, Gill (1980), Lau and Lim (1982), Zebiak (1982), Lim and Chang (1983), Heckley and Gill (1984), Phlips and Gill (1987), all based on linear equatorial beta-plane equations. Hirst (1986) has coupled such a model to a shallow-water ocean to investigate free coupled modes. Webster (1972) has used linear continuous and two-layer models with prescribed heating.

Specifying the heating begs the question of why sources and sinks are located at particular spots, however. In practice, the main sources are due to latent heat release in the troposphere in regions of deep convection. The fuel for such heat sources is the moisture which is carried to the source by a field of motion which itself depends on the strength and location of the source. Understanding the dynamics requires an appreciation of the interdependence between the moisture field and the flow field. In a series of papers, Gill (1982b, 1982c, 1985) has developed the simplest possible model for examining this relationship. A more complex model with active moisture can be found in Lorenz (1984), and the two-level model by Held and Suarez (1978) is a further step toward the full physics of a general circulation model.

The simplicity of the Gill model stems from assuming a fixed baroclinic structure in the vertical which leads to the linearized shallow-water equations. With this structure, flow in the lower troposphere is oppositely directed to that in the upper troposphere, with zero horizontal velocity at mid-level. The vertical velocity is maximum at mid-level, as are thermal perturbations produced by heating. Simplicity in the moisture equation comes from the assumption that moisture is confined to the lower troposphere, so the moisture flux is determined by the low-level winds and the total column moisture. Thus the full set of equations consists of the shallow-water equations plus a dynamic moisture equation and a condition (namely that a saturation level is reached) for precipitation and latent heat release. The equations involve only horizontal position and time, as vertical

structure is specified. Recently Weare (1986a, b) has presented results from a similar model wherein steady states were calculated by iteration of the latent heating and the circulation thus produced.

The model needs some representation of the forcing which would occur even in the absence of latent heat release. In particular, a simple representation is required of the heating that takes place due to the sun shining on the ocean and setting off the chain of processes that determines the sea surface temperature (s.s.t.) and the structure of the atmosphere above it. In the simple model this heating can only be represented by a source term in the thermal equation. This term defines a temperature θ_s towards which the mid-level temperature perturbation θ is driven. The equations are linearized about a state of rest with horizontally uniform stratification.

The purpose of this paper is to determine the response of the moist model for different prescribed fields of θ_s. For instance, what properties of the θ_s distribution determine whether the response circulation is predominantly Hadley-like or Walker-like? For answering such questions the precise relationship between θ_s and fields one might observe is not important. However, it is clear that θ_s will be closely related to s.s.t., i.e. that there are thermal processes which will tend to make the mid-level temperature field in the tropics vary with latitude and longitude in a similar way to the surface field. For instance, a constant lapse rate between the surface and mid-levels would require the two fields to be identical. In a numerical experiment by Rowntree (1972) using a general circulation model of the atmosphere with a specified s.s.t. anomaly, a direct relation between mid-level heating and s.s.t. was apparent.

Following a detailed presentation of the model equations in section 2, we examine in section 3 the response to θ_s distributions based on observed s.s.t. fields for the tropical Pacific Ocean, for January and July conditions. Circulation and precipitation patterns quite like actual ones are found.

In sections 5 and 6 some simple examples are examined for zonally symmetric flow with and without precipitation, showing how latent heat release intensifies and narrows regions of upward motion. The dependence of precipitation location and magnitude on the saturation moisture level is also examined analytically. Departures from zonal symmetry are similarly treated in sections 7 and 8. We find that it is a good approximation to neglect Rayleigh friction while retaining Newtonian cooling in the dynamics of zonally varying flow. The influence of zonal variations on precipitation patterns is discussed further in section 9, with reference to Hadley-type and Walker-type circulation.

2. THE MODEL AND THE GOVERNING EQUATIONS

In this section the basic equations are derived in some detail using vertical modes. Further discussion can be found in Gill (1982b).

(a) Dimensional form

We will consider small perturbations from a state of rest with potential temperature $\theta_o(z)$, density $\rho_o(z)$, pressure $p_o(z)$, and buoyancy frequency N defined by

$$N^2 = (g/\theta_o)d\theta_o/dz. \tag{2.1}$$

For simplicity the model atmosphere is bounded by rigid horizontal planes at $z = \pi H$ and at the sea surface $z = 0$. An equatorial beta plane is used with (x, y) as distance (eastward, northward) and Coriolis parameter

$$f = \beta y. \tag{2.2}$$

The linear momentum equations are

$$u_t - fv = -p_x/\rho_0 + \text{dissipation} \tag{2.3a}$$

$$v_t + fu = -p_y/\rho_0 + \text{dissipation} \tag{2.3b}$$

where p is the pressure perturbation from p_0.

The atmosphere is taken to be incompressible, as only baroclinic motion will be considered, so

$$u_x + v_y + w_z = 0. \tag{2.4}$$

Pressure and potential temperature perturbations p and θ are related through hydrostatic balance by

$$(p/\rho_0)_z = g\theta/\theta_0. \tag{2.5}$$

A second term $(N^2/g)p/\rho_0$ has been neglected on the right as it is relatively small for the scales of interest.

The linear temperature perturbation equation is

$$\theta_t + w\theta_0 N^2/g = Q_s + Q + \text{dissipation} \tag{2.6}$$

where Q represents latent heating. The term Q_s represents other forms of heating which in this simple model takes the form of Newtonian cooling

$$Q_s = (\theta_s - \theta)/\tau \tag{2.7}$$

to force θ towards θ_s on a timescale τ. Here θ_s is prescribed with the same horizontal pattern as the underlying sea surface temperature. Effectively we assume that, apart from latent heating, thermodynamic processes are spatially uniform so in the absence of motion this model atmosphere would have the same vertical lapse rate everywhere and θ would adopt the same pattern as the s.s.t.

A vertically integrated form of the moisture equation will be used to determine the latent heating. For specific humidity s the total moisture in a column of air is

$$q = \int_0^{\pi H} s\, dz/\rho_w. \tag{2.8}$$

Here ρ_w is the density of water, so q is expressed as the depth of precipitable water. We assume that water vapour is concentrated near the sea surface, so the moisture flux is approximately

$$\int_0^{\pi H} \mathbf{u}s\, dz = q\mathbf{u}_s \tag{2.9}$$

where $\mathbf{u}_s = (u_s, v_s)$ is the horizontal velocity at $z = 0$. Then the moisture balance is

$$q_t + P = -\nabla \cdot (\mathbf{u}_s q) + E + \text{diffusion}. \tag{2.10}$$

Evaporation in the form

$$E = (\hat{q} - q)/\tau \tag{2.11}$$

drives the moisture content q toward a saturation value $\hat{q}$, with the same timescale as in Eq. (2.7) for convenience. The term $\hat{q}$ can be related to surface temperature, but as such variations were found to have only a qualitative effect for the cases considered we will henceforth take $\hat{q}$ to be constant.

Precipitation at rate P occurs when q is tending to increase beyond some threshold value, here taken to be $\hat{q}$. All excess moisture is precipitated. This can be expressed mathematically as

$$q_t = 0, \qquad P = R \qquad\qquad (2.12a)$$

when $q = \hat{q}$ and $R > 0$, else

$$q_t = R, \qquad P = 0 \qquad\qquad (2.12b)$$

where R is the right-hand side of (2.10).

(b) Vertical structure

The equations (2.3) to (2.6) can be separated into vertical modes. For simplicity we take N to be constant so the modes are sinusoidal. For the first baroclinic mode

$$\mathbf{u} = \tilde{\mathbf{u}}(x, y, t) \cos(z/H) \qquad\qquad (2.13a)$$

$$w = \tilde{w} \sin(z/H) \qquad\qquad (2.13b)$$

$$(\theta, \theta_s, Q) = (\tilde{\theta}, \tilde{\theta}_s, \tilde{Q}) \sin(z/H)\, \theta_0(z)/\theta_{00} \qquad\qquad (2.13c)$$

$$p = \tilde{p} \cos(z/H) \rho_0(z)/\rho_{00} \qquad\qquad (2.13d)$$

where θ_{00} and ρ_{00} are characteristic values of θ_0 and ρ_0. Pressure perturbations and horizontal velocity are largest at upper and lower levels with opposite sign, whereas vertical motion and temperature perturbations are largest at mid-level as shown in Fig. 1.

Higher-order modes will be neglected, though the modes are coupled via the precipitation, because latent heating mainly forces the first baroclinic mode. This is a reasonable approximation for the tropics where deep convection produces maximum heating at mid-levels.

From Eq. (2.5) horizontal pressure and temperature variations are related by

$$\tilde{p}/\rho_{00} = -gH\,\tilde{\theta}/\theta_{00}\,. \qquad\qquad (2.14)$$

Other equations for horizontal structure are

$$\tilde{u}_t - f\tilde{v} = gH\tilde{\theta}_x/\theta_{00} + \text{dissipation} \qquad\qquad (2.15a)$$

$$\tilde{v}_t + f\tilde{u} = gH\tilde{\theta}_y/\theta_{00} + \text{dissipation} \qquad\qquad (2.15b)$$
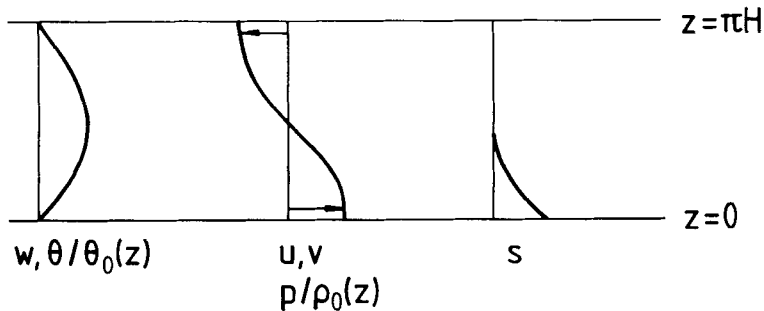

Figure 1.   The vertical structure assumed in the model. Potential temperature perturbation θ and vertical velocity w are largest at the mid-troposphere level. Horizontal velocity u, v and pressure perturbation p have largest and opposite values at lower and upper levels. Specific humidity s is concentrated at low levels.

$$\tilde{u}_x + \tilde{v}_y + \tilde{w}/H = 0 \tag{2.16}$$

$$\tilde{\theta}_t + wN^2\theta_{oo}/g = (\tilde{\theta}_s - \tilde{\theta})/\tau + \tilde{Q} + \text{dissipation} \tag{2.17}$$

and the moisture equation becomes

$$q_t + P = -\nabla \cdot (\tilde{u}q) + (\hat{q} - q)/\tau + \text{diffusion.} \tag{2.18}$$

A relation between P and Q is needed to complete the model. By unresolved deep convection processes the condensation of water vapour contributing to P has some vertical distribution, projecting onto that of the first baroclinic mode for Q. The actual relation is complex; here we simply specify

$$Q = (L\rho_w/c_p\rho_{oo}H_o)P \tag{2.19}$$

where c_p is the specific heat of air, L is the latent heat of condensation, and H_o is a constant projection factor with units of height. If all latent heating goes into the first baroclinic mode then $H_o \approx 2H$.

From (2.15) to (2.17) the speed of the first baroclinic mode gravity waves is $C = NH$.

(c) Non-dimensional variables and equations

The equatorial Rossby radius, $a = (C/2\beta)^{1/2}$, is a natural length scale. The typical value $C = 50\,\mathrm{m\,s^{-1}}$ gives $a = 1000\,\mathrm{km}$, and a timescale a/C of a quarter of a day. We choose

$$\left.\begin{aligned}
(x, y, z) &= a[x^*, y^*, (H/a)z^*] \\
(\tilde{u}, \tilde{v}, \tilde{w}) &= C[u^*, v^*, (H/a)w^*] \\
t &= (a/C)t^* \\
(\tilde{\theta}, \tilde{\theta}_s, \tilde{Q}) &= \frac{C^2\theta_{oo}}{gH}[\theta^*, \theta_s^*, (C/a)Q^*] \\
(q, \hat{q}, P) &= \frac{C^2\theta_{oo}c_p\rho_{oo}H_o}{gHL\rho_w}[q^*, \hat{q}^*, (C/a)P^*] \\
f &= 2\beta af^*.
\end{aligned}\right\} \tag{2.20}$$

Then, dropping the asterisks used above to denote non-dimensional variables, the basic non-dimensional equations are

$$u_t - fv = \theta_x - \varepsilon u + \nu\nabla^2 u \tag{2.21a}$$

$$v_t + fu = \theta_y - \varepsilon v + \nu\nabla^2 v \tag{2.21b}$$

$$u_x + v_y + w = 0 \tag{2.22}$$

$$\theta_t + w = \varepsilon(\theta_s - \theta) + Q + \nu\nabla^2\theta \tag{2.23}$$

$$q_t + P = -\nabla \cdot (uq) + \varepsilon(\hat{q} - q) + \nu\nabla^2 q \tag{2.24}$$

$$Q = P \tag{2.25}$$

where $f = \frac{1}{2}y$ and $\varepsilon = a/(C\tau)$. Laplacian dissipation and diffusion terms have been specified, along with Rayleigh friction with the same timescale as the Newtonian cooling.

(d) Static stability

The saturated moisture content $\hat{q}$ plays a very important role in determining the behaviour of the system. In a region of rain, where $q = \hat{q}$ is constant, (2.24) reduces to

$$P = \hat{q}w \qquad (2.26)$$

and the temperature equation (2.23) becomes

$$\theta_t + (1 - \hat{q})w = \varepsilon(\theta_s - \theta) + \nu\nabla^2\theta. \qquad (2.27)$$

The form of this equation is the same as in the dry region where $Q = 0$, except that the buoyancy restoring term w in (2.23) is replaced by $(1 - \hat{q})w$ in (2.27). The difference arises because latent heat release opposes the reduction of buoyancy due to upward motion, so the static stability is reduced in the wet region. The non-dimensional form (2.20) has been chosen such that moist static stability is zero when $\hat{q} = 1$.

The effect of this reduction was examined in Gill (1982b) and many interesting phenomena were found, such as propagating fronts and rainbands. Features propagate at unit speed in dry regions, but at speed $(1 - \hat{q})^{1/2}$ in wet regions.

When $\hat{q} > 1$ the system is locally unstable in wet regions: this corresponds to the vertical potential temperature gradient being moist unstable. Some solutions for a uniformly rotating atmosphere with $\hat{q} > 1$ were discussed in Gill (1982c) which correspond to hurricane-like disturbances with a 'moist Rossby radius' length scale equal to $(\hat{q} - 1)^{1/2}$ times the dry value. Equatorial numerical solutions with $\hat{q} > 1$ appear in Davey (1985).

Equatorial solutions with $\hat{q} \leqslant 1$ have been described in Gill (1985): in particular a zonally-symmetric solution with a feature corresponding to the intertropical convergence zone was obtained, and an analytic solution found for $\hat{q} = 1$.

For the large-scale tropical circulation problems studied in the following sections we take $\hat{q} = 8/9$ unless otherwise specified.

3. NUMERICAL RESULTS FOR 'JANUARY' AND 'JULY' SIMULATIONS FOR THE PACIFIC

The simple model was constructed as a means of improving understanding of moisture effects on the large-scale circulation in the tropics, so can it produce reasonable precipitation fields for the Pacific Ocean?

The model is for flow over the ocean only, and requires a sea surface temperature pattern as input. To achieve this, an equatorial beta-plane channel was set up with boundaries at $y = \pm 4$ (about $\pm 40°$ latitude) and with periodic east–west boundary conditions—effectively a periodically repeated Pacific Ocean with no land or other oceans in between. The length of the model Pacific is 16 units (about $160°$ longitude). The forcing temperature θ_s was set by specifying a western meridional profile $\theta_W(y)$ to apply at $x = -4$, and an eastern profile $\theta_E(y)$ for $x = +4$, with periodic behaviour in between:

$$2\theta_s = \theta_E + \theta_W + (\theta_E - \theta_W)\sin(\pi x/8). \qquad (3.1)$$

The eastern and western profiles were chosen by constructing analytic curves with similar properties to the observed ones. For the western Pacific,

$$\theta_W = 1 - (y - Y)^2(Y^2 + 2yY + 16)/(Y^2 + 16)^2 \qquad (3.2)$$

with $Y = 0$ for January and $Y = 1.5$ for July. This curve has a maximum of one at $y = Y$. The eastern profile is

$$\theta_E = 0.6(1 - y^2/16) + A\exp\{-(y - 1)^2\} \qquad (3.3)$$

with $A = 0{\cdot}1$ for January and $A = 0{\cdot}3$ for July. The first term in (3.3) gives a parabolic shape vanishing at $y = \pm 4$ and with a maximum of $0{\cdot}6$ at the equator. The second term adds a Gaussian bump centred at $y = 1$. Overall, the maximum eastern value is $0{\cdot}67$ in January and $0{\cdot}87$ in July.

Equations (2.21)–(2.25) were solved by numerical integration, time-stepping on a finite-difference spatial C-grid with spacing of half a Rossby radius in each direction. To ensure numerical stability the Laplacian diffusion of u, v, θ and q was included. Results are shown for the parameter values $\hat{q} = 8/9$, $\varepsilon = 0{\cdot}1$, and $\nu = 0{\cdot}025$. Integration is carried out to $t = 60$, by which time the response is effectively steady.

Figure 2 shows the temperature patterns θ_s that force the motion. Precipitation rate P, dryness $D = 1 - q/\hat{q}$, low-level velocity and mid-level potential temperature perturbation θ appear in Figs. 3–6 for January and July.

In January the forcing field is characterized by having the maximum temperature on the equator in the west, with a relatively large east–west temperature contrast ($0{\cdot}33$ difference between eastern and western maxima). As shown in Fig. 3(a), the rainfall is
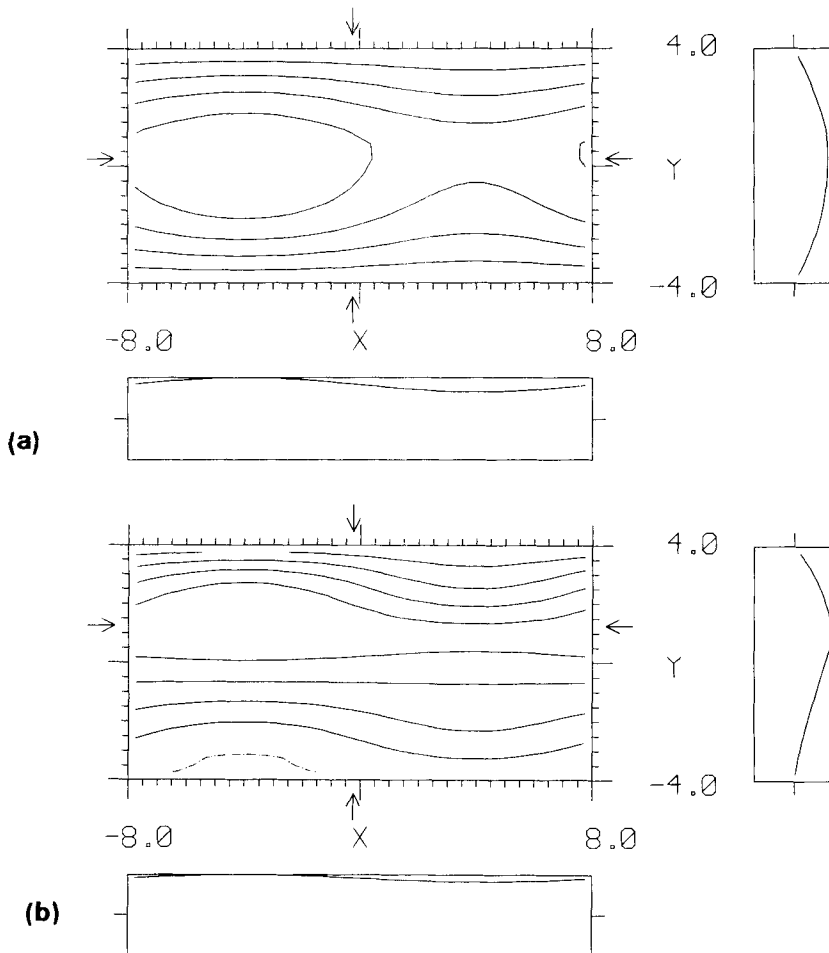

(a)

(b)

Figure 2.   Forcing temperature θ_s has the same horizontal pattern as tropical Pacific sea surface temperatures for (a) January with minimum value $0{\cdot}73$, max $= 1{\cdot}0$; and (b) July with min $= -0{\cdot}02$, max $= 1{\cdot}0$. Contour interval (c.i.) $=$ max/5. Zonal and meridional cross-sections indicated by arrows are shown below and to the right of the contour maps. Distance units are equatorial Rossby radii, about $10°$ of latitude or longitude.
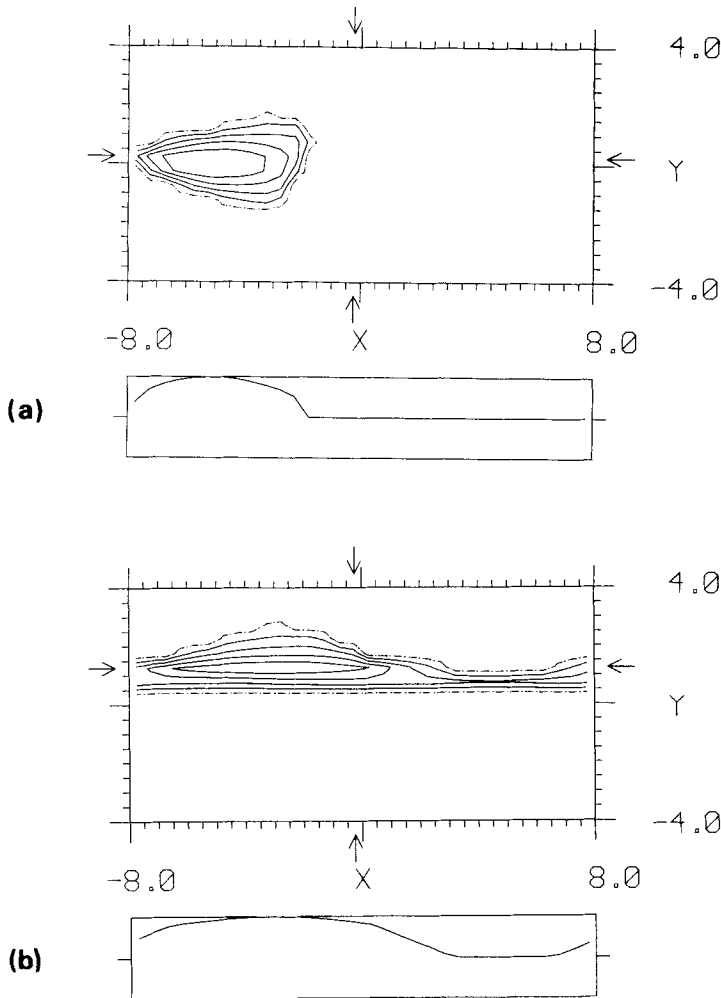
Figure 3. Precipitation P at time $t = 60$ for $\varepsilon = 0\cdot1$, $\nu = 0\cdot025$, $\hat{q} = 8/9$. Non-dimensionally P is equal to the latent heating rate Q. The zero contour is dash-dotted. (a) January with max $= 0\cdot11$; (b) July with max $= 0\cdot11$. c.i. $= \text{max}/5$.

centred over the warmest ocean, thereby giving a response like the winter monsoon with heavy precipitation over the Indonesian region. The driest regions in Fig. 4(a) (which mark the zones of maximum downward motion) are an extensive area on the eastern side south of the equator and a less extensive area on the eastern side north of the s.s.t. maximum. The moister zone has a narrow westward extension along the equator from its centre over Indonesia, and broader extensions on the east to both the north-east and south-east. The south-east extension is a sharper feature which can be related to the South Pacific convergence zone. The main contrasts are between east and west, giving the impression of a Walker cell type of structure.

In July the forcing field is rather different, with maximum values in the northern hemisphere near $y = 1$. The precipitation (Fig. 3(b)) is again found over the warmest ocean, but is now very elongated east–west to form an extensive intertropical convergence zone. The driest area in the tropics in Fig. 4(b) is now at the same longitude as the warmest water, in the west, but located in the opposite hemisphere to the precipitating
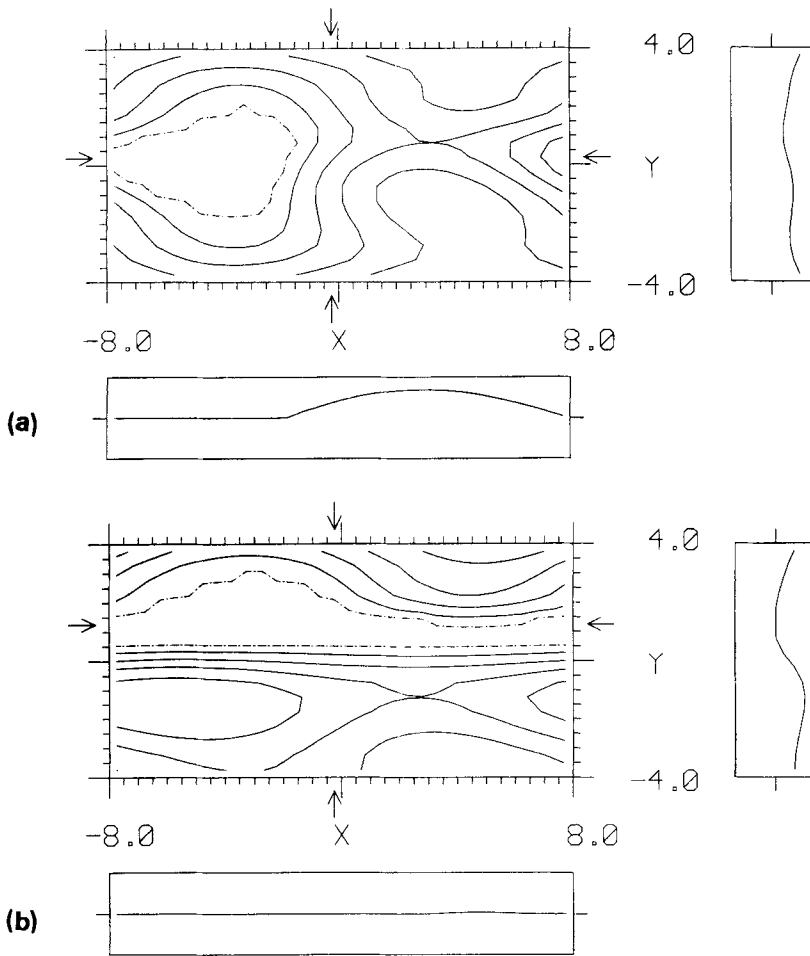
Figure 4. Dryness $1 - q/\hat{q}$ at time $t = 60$, for $\varepsilon = 0 \cdot 1$, $\nu = 0 \cdot 025$, $\hat{q} = 8/9$. Within the dash-dotted zero contour $q = \hat{q}$ and precipitation will occur where there is low-level convergence. (a) January with max $= 0 \cdot 15$; (b) July with max $= 0 \cdot 22$. c.i. $= \mathrm{max}/5$.

region. Thus a Hadley-like circulation is apparent with rising motion over the warmest water and a descending branch in the southern hemisphere.

The low-level winds shown in Fig. 5 are dominated by easterly trade winds off the equator, being associated with the thermal wind due to the north–south temperature gradient. In January the trades extend right across the equator in the central Pacific, where they reach their strongest values and constitute the low-level branch of the Walker circulation. To the west of Indonesia there are very strong westerly monsoon winds directed into the zone of heavy precipitation.

In July the southern hemisphere trades are strongest and a marked cross-equatorial flow can be seen in Fig. 5(b), particularly in the west, providing the low-level branch of the Hadley cell. This flow veers strongly as it crosses the equator and becomes westerly in the northern hemisphere. There is a region of very weak flow at about 15°N ($y = 1 \cdot 5$) where a very shallow trough separates these westerlies from the easterlies further north.

The maps of mid-level potential temperature perturbation θ in Fig. 6 are relatively featureless, showing much less zonal contrast than θ_s and with no clear indication of the
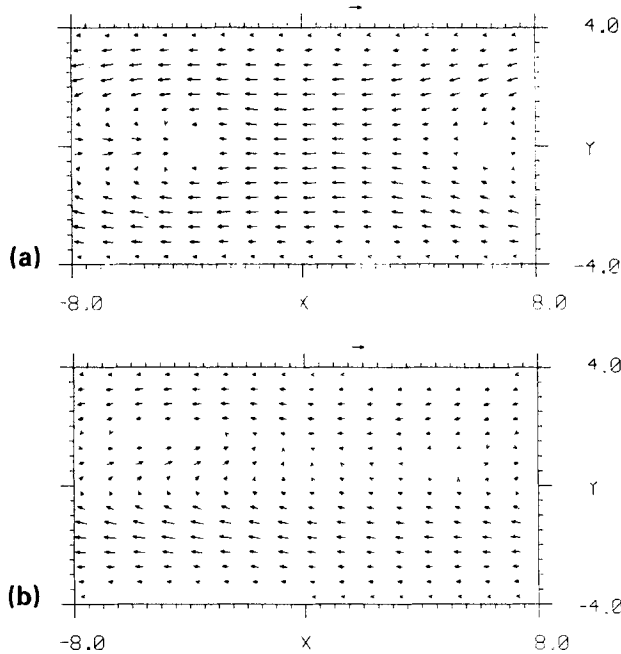
Figure 5. Low-level wind (u, v) at time $t = 60$, for $\varepsilon = 0\cdot1$, $v = 0\cdot025$, $\hat{q} = 8/9$. Upper-level wind is oppositely directed. (a) January with max speed $= 0\cdot20$; (b) July with max $= 0\cdot29$. The arrows at the top of the diagrams correspond to the maximum speed.

precipitation regions. Maps of vertical velocity (not shown) are dominated by strong ascent where it is raining, with much weaker downward motion elsewhere.

Obviously a simple model like the one described will not give a perfect simulation of observations, but the patterns are very much like real ones and this encourages the belief that ideas stemming from further analysis will be useful for understanding the real atmosphere. With the model it is easy, for example, to vary east–west contrasts in the forcing s.s.t. field to see at what point Walker cell characteristics start to become more pronounced than those of a Hadley cell. Analysis can be done to determine the effects of various parameters. The remainder of the paper will be devoted to such questions, beginning with the simplest case of zonally symmetric flow.

4. EQUATIONS FOR STEADY FLOW

In this section the basic equations are manipulated into forms more amenable to solution, for use in later sections. The reader interested in results can proceed to section 5, and refer back to this section as necessary.

Neglecting the Laplacian terms that were included for time-stepping numerical stability, (2.21) and (2.23) reduce for steady flow to

$$-fv = \theta_x - \varepsilon u \tag{4.1}$$

$$fu = \theta_y - \varepsilon v \tag{4.2}$$

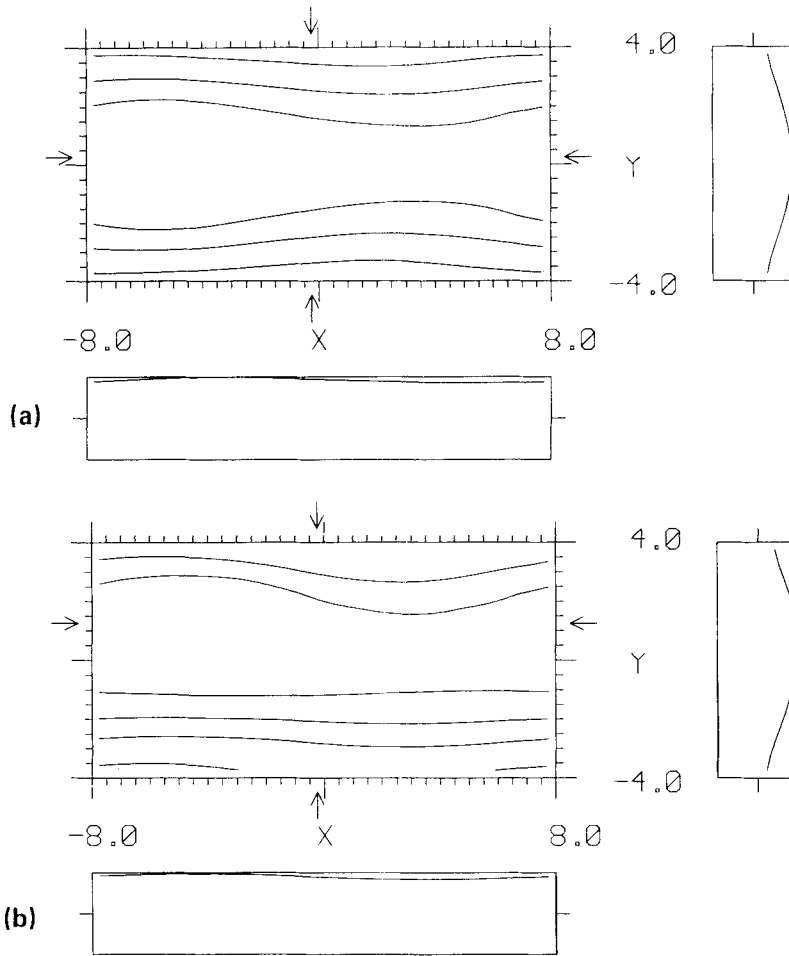$$\alpha w = \varepsilon(\theta_s - \theta) \tag{4.3}$$

Figure 6. Mid-level potential temperature perturbations θ at time $t = 60$ (about 15 days), effectively a steady state, for the model with $\varepsilon = 0 \cdot 1$, $\nu = 0 \cdot 025$, $\hat{q} = 8/9$. (a) January with min $= 0 \cdot 29$, max $= 0 \cdot 86$; (b) July with min $= 0 \cdot 15$, max $= 0 \cdot 86$. c.i. $=$ max/5.

where

$$\alpha(x, y) = \begin{cases} 1 & \text{no precipitation} \\ 1 - \hat{q} & \text{with precipitation} \end{cases} \tag{4.4}$$

represents the spatially-varying static stability. The moisture equation (2.24) gives

$$q = \begin{cases} \hat{q} - \nabla \cdot (\mathbf{u}q)/\varepsilon & \text{no precipitation} \\ \hat{q} & \text{with precipitation.} \end{cases} \tag{4.5}$$

In view of the conditions that $v = 0$ at the northern and southern boundaries it is simplest to solve an equation for v alone. From (4.1)–(4.3) this is

$$\alpha(\varepsilon\nabla^2 v + \beta v_x) - \varepsilon(\varepsilon^2 + f^2)v = \varepsilon f \theta_{sx} - \varepsilon^2 \theta_{sy}. \tag{4.6}$$

(Remember that $f = \beta y$ with $\beta = \frac{1}{2}$, and that θ_s is prescribed.)

Although (4.6) is linear in the regions with and without precipitation separately, it is nonlinear with regard to the position of these regions as expressed by $\alpha(x, y)$ and must usually be solved by numerical means. Once v and α are known, u and θ can be found easily by solving

$$\alpha u_{xx} - \varepsilon^2 u = -\alpha v_{xy} - \varepsilon \theta_{sx} - f\varepsilon v \qquad (4.7)$$

$$\alpha \theta_{xx} - \varepsilon^2 \theta = -\alpha f v_x - \varepsilon^2 \theta_s - \alpha \varepsilon v_y \qquad (4.8)$$

latitude by latitude.

The curl of (4.1) and (4.2) gives

$$-\beta v + fw = \varepsilon(v_x - u_y) \qquad (4.9)$$

which for vanishing Rayleigh friction reduces to the Sverdrup relation

$$\beta v = fw. \qquad (4.10)$$

This relation implies that upward motion is accompanied by poleward low-level flow, and in section 7 this is shown to be a good approximation for the zonally varying component of flow.

Some general statements can be made about the location of precipitation in this model. Within a wet region $P = \hat{q}w > 0$ and vertical motion is upward. At the boundary between wet and dry regions the stability parameter α is discontinuous, but w, θ and θ_s are continuous, so (4.3) requires $w = 0$ there. In summary,

$$\alpha = 1, \qquad w < 0, \qquad \theta > \theta_s \qquad \text{in dry region}$$

$$w = 0, \qquad \theta = \theta_s \qquad \text{at boundary of wet region}$$

$$\alpha = 1 - \hat{q}, \qquad w > 0, \qquad \theta < \theta_s \qquad \text{in wet region.}$$

The constraint that there be zero net vertical motion requires $w > 0$ somewhere (except in the static $w \equiv 0$ case), so in this steady model it must rain somewhere, but not everywhere.

From (4.1)–(4.3) an equation for θ alone can be obtained:

$$\alpha[-\varepsilon(\varepsilon^2 + f^2)\nabla^2\theta + (\varepsilon^2 - f^2)\beta\theta_x + 2\varepsilon f\beta\theta_y] = \varepsilon(\varepsilon^2 + f^2)(\theta_s - \theta). \qquad (4.11)$$

Hence $\theta_s > \theta$ where θ has a local maximum, so it must rain at such a point. Physically this location is a low-level low pressure centre, associated with low-level convergence and rising motion. Further, we can deduce that the absolute maximum of θ_s must lie inside a region of precipitation. For this model with θ_s having the same pattern as s.s.t. it always rains over the position of maximum s.s.t.

It is sometimes useful to define a 'latent heating forcing temperature' by

$$\theta_L = P/\varepsilon = \begin{cases} \hat{q}w/\varepsilon = (\theta_s - \theta)\hat{q}/(1 - \hat{q}) & \text{wet region} \\ 0 & \text{dry region.} \end{cases} \qquad (4.12)$$

Then (4.3) can be re-expressed as

$$w = \varepsilon(\theta_s + \theta_L - \theta). \qquad (4.13)$$

Thus the solution to a model with rain and forcing θ_s can be expressed as the superposition of linear dry models with forcing θ_s and θ_L. Generally θ_L is not known in advance, but it can be parametrized to obtain approximate solutions.

5. ZONALLY SYMMETRIC STEADY SOLUTIONS: DRY CASE

When no rain is allowed in the model and there is no east–west variation some useful simple solutions can be obtained. In this case the static stability parameter $\alpha = 1$ everywhere and the steady equation (4.6) for v reduces to

$$v_{yy} - (f^2 + \varepsilon^2)v = -\varepsilon\theta_{sy} \qquad (5.1)$$

where $f = y/2$. In terms of v other variables are

$$u = fv/\varepsilon \qquad (5.2)$$

$$w = -v_y \qquad (5.3)$$

$$\theta = \theta_s + v_y/\varepsilon. \qquad (5.4)$$

Equation (5.1) can be easily solved numerically in any given case. The term ε^2 is usually small: certainly for $\varepsilon \leqslant 0\cdot1$ results with this term neglected are almost identical to those with ε^2 retained. Hence we shall use the approximate form

$$v_{yy} - f^2v = -\varepsilon\theta_{sy} \qquad (5.5)$$

which has analytic solutions. With $\theta_s \sim 1$, the ordering of the dependent variables is

$$v \sim \varepsilon, \quad w \sim \varepsilon, \quad \theta \sim 1, \quad u \sim 1.$$

As an archetype of the behaviour to be expected, an analytic solution (described in appendix A) can be found when the surface temperature has the parabolic shape

$$\theta_s = 1 - (y/b)^2. \qquad (5.6)$$

Profiles of u, v, w and θ for the case $b = 4$ are shown in Fig. 7, along with streamlines and normal flow in a meridional section. There are low-level easterly jets north and south of the equator, with u vanishing at the equator as required by Eq. (5.2). Meridional flow is equatorward at low level, giving broad rising motion around the equator.

Another useful case to consider is the response to forcing at one latitude only, i.e. for the heat source

$$\theta_s = \delta(y - y_o). \qquad (5.7)$$

(See appendix A for details.)

Profiles of u, v and θ are given in Fig. 8 for $y_o = 0$ and $y_o = 1$. As we would expect, low-level meridional flow is toward the heat source, with a discontinuity at y_o. Except for the case $y_o = 0$ there is a corresponding discontinuity in the zonal flow, with westerlies between y_o and the equator and easterlies elsewhere. The discontinuity in u is caused by the discontinuity in v, due to the balance of damping and Coriolis terms as described by Eq. (5.2). Temperature is positive and continuous everywhere, and w is negative everywhere except at $y = y_o$ where there is a positive spike such that there is zero net vertical velocity. (Circulation in a meridional plane can be seen in Fig. 11.18 of Gill (1982a) for a similar example.) Note that the strongest downward motion is adjacent to y_o.

6. ZONALLY SYMMETRIC STEADY SOLUTIONS: MOIST CASE

When precipitation is included the problem is more difficult because the boundary of the wet region is not known beforehand. From Eq. (4.6) the basic equation is

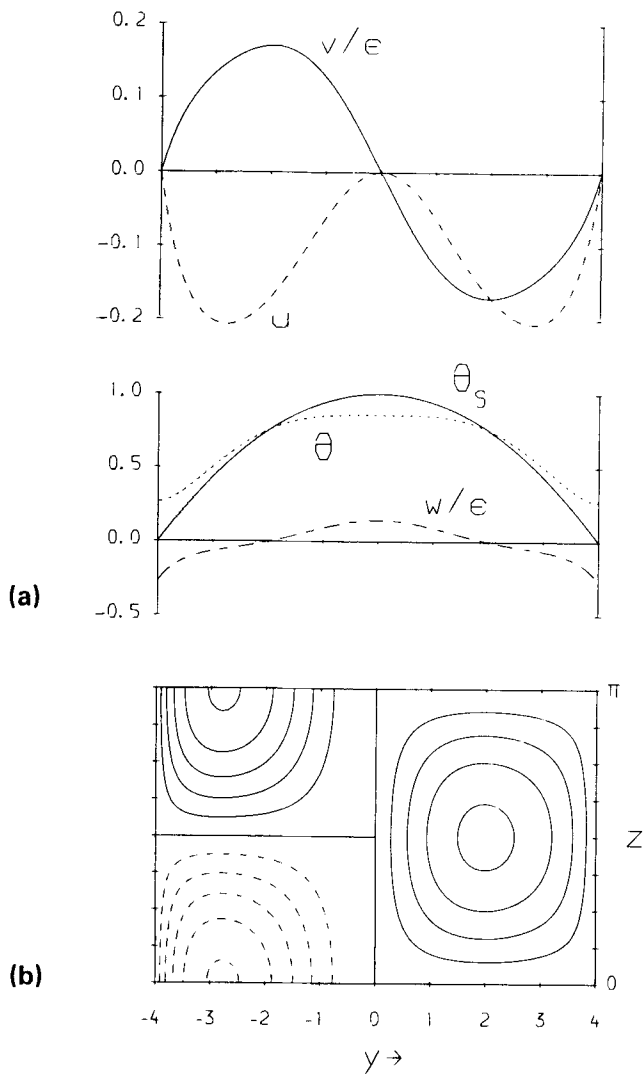$$\alpha v_{yy} - (\varepsilon^2 + f^2)v = -\varepsilon\theta_{sy} \qquad (6.1)$$

Figure 7. The analytic response to the forcing temperature $\theta_s = 1 - (y/4)^2$ for the steady zonally symmetric model with no latent heating. (a) Meridional profiles of θ_s, mid-level potential temperature perturbation θ and vertical velocity w/ε, and low-level velocity components u and v/ε. (b) y–z plane showing the zonal flow u (south of the equator) and streamlines for the meridional flow (v, w) north of the equator. These patterns are symmetric about the equator. Negative contours are dashed.

where $\alpha(y)$ is given by (4.4). We restrict attention to moist stable cases so $\hat{q} < 1$ and α is positive everywhere. Once v is known, u and w follow from (5.2) and (5.3), while (5.4) is modified to

$$\theta = \theta_s + \alpha v_y/\varepsilon. \tag{6.2}$$

Boundary conditions are

$$v = 0 \quad \text{at } y = \pm b \tag{6.3a}$$

and, because $w = 0$ at the boundary of the wet region,

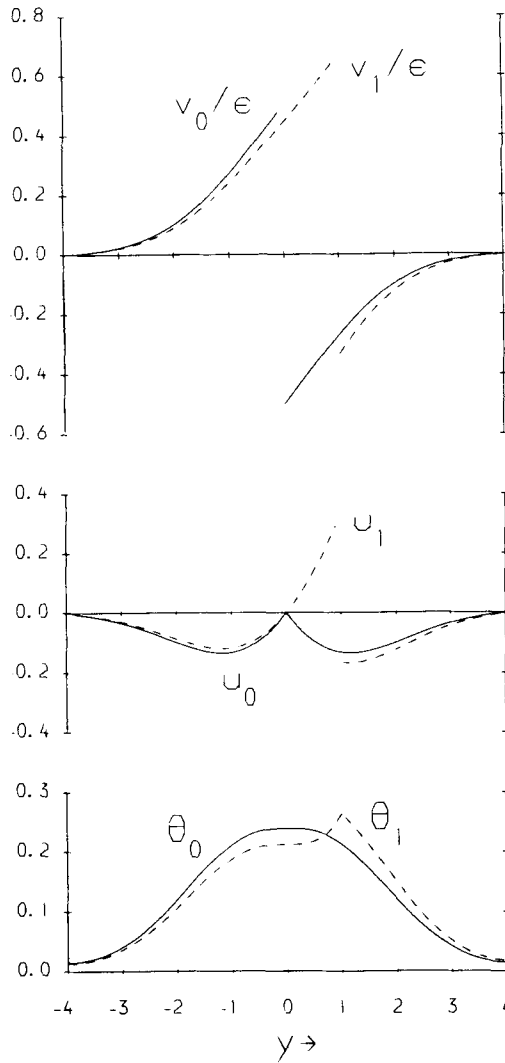$$v_y = 0 \quad \text{at the precipitation boundary.} \tag{6.3b}$$

Figure 8.   The analytic response to the forcing temperature $\theta_s = \delta(y - y_o)$ concentrated along the line $y = y_o$, for the steady zonally symmetric model with no latent heating. Meridional profiles of mid-level potential temperature perturbation θ and low-level velocity components u and v/ε are shown for $y_o = 0$ (solid) and $y_o = 1$ (dashed). Vertical velocity w is related to θ by $w/\varepsilon = -\theta$ for $y \neq y_o$: balance of upward and downward motion is provided by a spike in w at y_o.

(a)   Numerical results

Equation (6.1) can be solved numerically as a boundary value problem. Solutions for the parabolic profile (5.6) are shown in Fig. 9 for $\hat{q} = 8/9$, $\varepsilon = 0.1$, and $b = 4$. Compared with the dry case in Fig. 7 we see that there is larger upward motion over a narrower region when latent heating is included. This effect becomes more pronounced as $\hat{q} \rightarrow 1$ and moist static stability decreases.

The quartic profile

$$\theta_s = 1 - (y/b)^4 \tag{6.4}$$

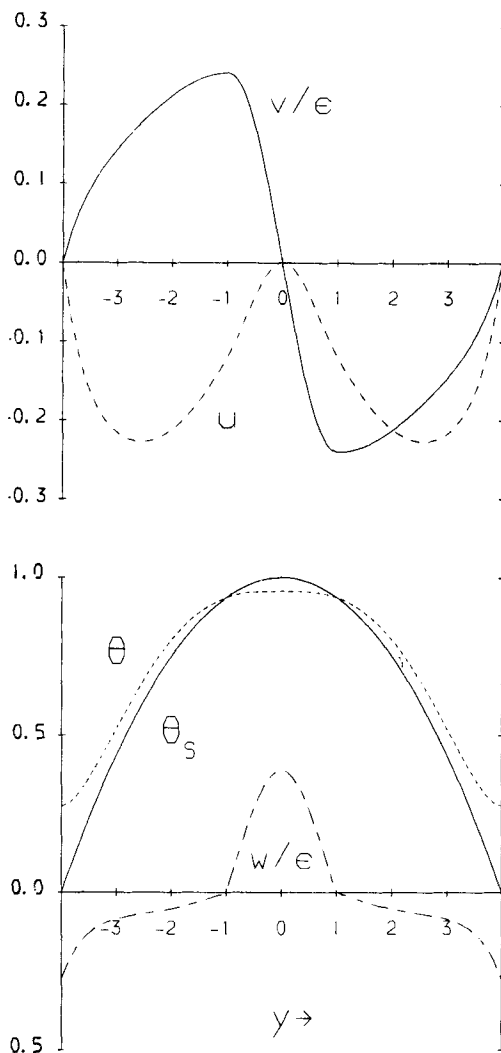was used to produce the results in Fig. 10, using the same parameters. The flatter shape

Figure 9.   The response to the forcing temperature $\theta_s = 1 - (y/4)^2$ for the steady zonally symmetric model with latent heating, for $\varepsilon = 0\cdot1$, $\hat{q} = 8/9$. Meridional profiles of θ_s, mid-level potential temperature perturbation θ and vertical velocity w/ε, and low-level horizontal velocity components u and v/ε are shown. Precipitation $P = \hat{q}w$ occurs where $w > 0$.

of θ_s around the equator in this case leads to a much wider wet region than for parabolic θ_s. Upward motion is weak however, and the net precipitation is nearly half that found for parabolic θ_s.

The net precipitation per unit zonal distance can be written as

$$P_{TOT} = \int_{-b}^{b} P \, dy = \int_{y_-}^{y_+} \hat{q}w \, dy = -\hat{q}(v_+ - v_-) \tag{6.5}$$

where subscripts $+$ and $-$ indicate values at the northern and southern edges of the rainband. (Low-level convergence into this region requires $v_+ < v_-$.) Both P_{TOT} and the width $y_+ - y_-$ are plotted in Fig. 11 for the parabolic and quartic cases, along with the
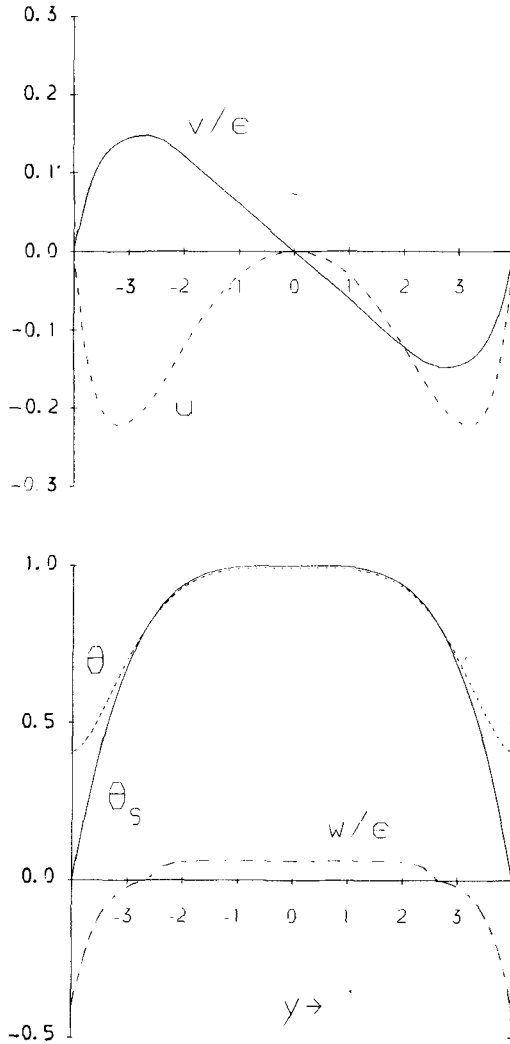
Figure 10.   As Fig. 9, but for the quartic forcing $\theta_s = 1 - (y/4)^4$.

estimates described below. As $\hat{q} \rightarrow 1$, P_{TOT} increases to a limiting value and $y_+ - y_-$ decreases toward zero. In the quartic case the decrease in width is gradual until $\hat{q}$ is very close to 1: the numerical method was not adequate to capture the sudden decrease toward zero.

(b)   Analytic estimates for parabolic θ_s

Some analytic progress can be made, and is described here for the parabolic forcing case as useful information about the parameter dependence of precipitation location and amount can thus be obtained.

As described in section 4 precipitation must occur at the location y_0 of the maximum of θ_s. As $\hat{q} \rightarrow 1$ the wet region shrinks toward this point. Hence as a first estimate we suppose that it rains only at y_0, and solve the dry region equation (5.5) for $y \neq y_0$ with boundary conditions (6.3). The result (see appendix B) is equivalent to the linear
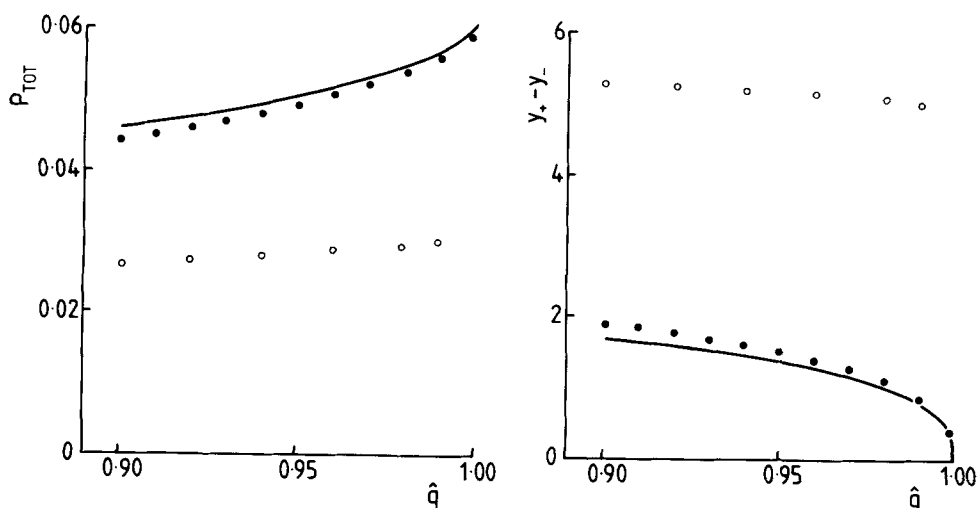
Figure 11.   Total precipitation P_{TOT} per unit zonal distance, and the width $y_+ - y_-$ of the precipitation region, for various values of $\hat{q}$. The solid lines are estimates and solid circles correspond to numerical solutions of the exact equations for forcing $\theta_s = 1 - (y/4)^2$. Open circles shown numerical solutions with $\theta_s = 1 - (y/4)^4$.

superposition of dry models with θ_s and with a point source representing the latent heating. The precipitation estimate equation (B3) thus obtained is, for $b = 4$,

$$P_{\mathrm{TOT}} = 0 \cdot 61\varepsilon \tag{6.6}$$

valid for $\hat{q} \to 1$.

This estimate can be extended to small values of $1 - \hat{q}$ by allowing the wet region to have finite width and matching an approximate solution in this region to the dry region, as described in appendix B. Figure 12 shows v_+ as a function of the position y_+ of the northern boundary of the wet region using Eq. (B2): as y_+ increases the magnitude of v_+ $(=-v_-)$ decreases. Hence the net precipitation must decrease from the limit (6.6) as $\hat{q}$ decreases from 1 and the width of the wet region increases.

Values of P_{TOT} and width $y_+ - y_-$ for varying $\hat{q}$ are included in Fig. 11, showing good agreement with the corresponding numerical solutions. The analytic solution shows that net precipitation depends linearly on the damping parameter ε, while the location of the wet region is independent of ε. For small $1 - \hat{q}$ we have from (B6) an explicit expression for the dependence of precipitation location on $\hat{q}$:

$$y_+ = 1 \cdot 94(1 - \hat{q})^{1/3}. \tag{6.7}$$

7.   Zonally varying steady solutions with no latent heating

In the absence of latent heating the model is linear, so zonally varying and zonally symmetric components can be determined separately. For small friction we show in this section that the dynamics of the zonal variations is quite different from that of the zonal average.

A zonal average will be denoted by an overbar, and departures are indicated by primes. From Eq. (4.6) for v we find that $\bar{v}$ and v' are both $O(\varepsilon)$ when θ_s is $O(1)$. If terms $O(\varepsilon^2)$ are neglected then (4.6) reduces to

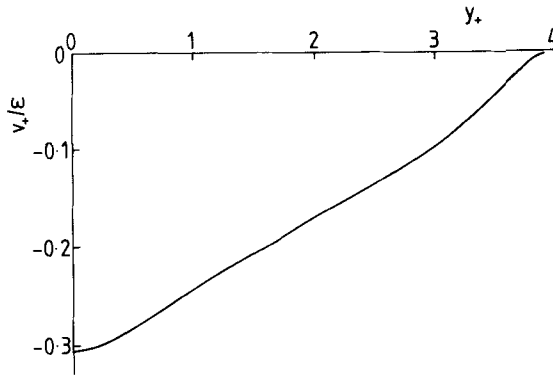$$\beta v'_x = \varepsilon f \theta'_{sx} \tag{7.1a}$$

Figure 12.   Meridional low-level velocity v_+ at the northern edge y_+ of the precipitation region, for the zonally symmetric forcing $\theta_s = 1 - (y/4)^2$.

which on integrating with respect to x becomes

$$\beta v' = \varepsilon f \theta_s'. \tag{7.1b}$$

Similarly, (4.7) leads to

$$u_x' = -v_y' - \varepsilon \theta_s'$$
$$= -2\varepsilon(f\theta_{sy}' + \theta_s') \tag{7.2}$$

so u' is $O(\varepsilon)$, in contrast to $\bar{u}$ which is $O(1)$ as found in section 5. Equation (4.8) likewise gives

$$\theta_x' = -fv' = -2\varepsilon f^2 \theta_s' \tag{7.3}$$

so θ' is also $O(\varepsilon)$, again contrasting with $\bar{\theta}$ which is $O(1)$. Further, θ' vanishes on the equator according to (7.3), so very little zonal variation in potential temperature is expected near the equator.

From (4.3) we deduce to $O(\varepsilon)$ that

$$w' = \varepsilon \theta_s'. \tag{7.4}$$

Consistently, the Sverdrup relation

$$\beta v' = fw' \tag{7.5}$$

is a good approximation for the zonally varying flow.

The approximations (7.1)–(7.5) could alternatively have been derived by neglecting Rayleigh friction $\varepsilon \mathbf{u}$ and Newtonian cooling $\varepsilon \theta$ in the basic equations (4.1)–(4.3). In this limit (studied by Gill and Phlips (1986)) v' and w' are in phase with the forcing θ_s', whereas u' and θ' are out of phase with θ_s'. These phases are such that upward motion is fed by zonal low-level inflow, as in a Walker cell.

This 'no friction/no cooling' limit can be contrasted with the 'large friction' limit in which frictional and cooling terms dominate zonal variations when $\varepsilon \geqslant$ zonal wavenumber. In this 'large friction' limit each longitude behaves independently, and equations for v' etc. take the same form as those for $\bar{v}$ etc. in section 5. Then θ' is $O(1)$, and in phase with θ_s'. Upward motion is now balanced by meridional low-level convergence, as in a Hadley cell.

For the forcing used in section 3, zonal variations have wavenumber $k = \pi/8$ which is larger than the largest value of ε considered here, namely 0·1, so the 'no friction/no cooling' limit should be a reasonable approximation. However, we find that a better approximation is to neglect Rayleigh friction but not the Newtonian cooling. Then the approximate form of (4.6) is

$$\beta v'_x - \varepsilon f^2 v' = \varepsilon f \theta'_{sx}. \tag{7.6}$$

Near the equator there is little difference from Eq. (7.1a), but the factor f^2 makes the Newtonian cooling increasingly important away from the equator. (Rayleigh friction terms are not affected in this way, so their continued omission is consistent.)

For this 'frictionless' model equations (7.1b)–(7.4) are modified to

$$\beta v' = \varepsilon f(\theta'_s - \theta') \tag{7.7}$$

$$u'_x = -2\varepsilon[f(\theta'_s - \theta')_y + \theta'_s - \theta'] \tag{7.8}$$

$$\theta'_x = -2\varepsilon f^2(\theta'_s - \theta') \tag{7.9}$$

$$w' = \varepsilon(\theta'_s - \theta'). \tag{7.10}$$

The Sverdrup balance (7.5) still applies.

To illustrate the effect of these various approximations we use the Pacific forcing (3.1) for January. Amplitude and phase lag (relative to θ'_s) of u', v', w' and θ' are shown in Fig. 13 for the 'frictionless' and 'no friction/no cooling' estimates, along with the exact solution found by numerical methods. The forcing has the same phase at all latitudes. For the 'frictionless' case, the phase lag is $\pm\arctan(\varepsilon f^2/\beta k)$ for v', θ' and w', independent of the amplitude of the forcing.

Generally, amplitudes obtained from the 'frictionless' model are larger than for the exact calculation, and 'no friction/no cooling' amplitudes are larger still, while meridional structure is broadly the same in each case. The 'frictionless' model estimates phase lags much better than the 'no friction/no cooling' model. The approximations are poorest for the phase lags of θ' and v' near the equator; however, these quantities also have low amplitude there so the error is not significant. Phases are such that there is Walker-type circulation with low-level zonal flow into, and meridional flow away from, a maximum of θ'_s near the equator, where there is upward motion.

8. Steady zonally varying solutions: precipitation estimates

As in section 6, some simple precipitation estimates for the zonally varying model can be obtained by considering $\hat{q} \to 1$, because the wet region then shrinks to a small area around the known position (x_o, y_o) of the maximum value of the prescribed forcing θ_s. Matching approximate solutions in the wet and dry regions is difficult when the unknown boundary varies in two dimensions, so here we use a method for which θ is assumed constant (θ_c say) in the wet region. (The numerical results in section 3 suggest that this approximation is reasonable: more rigorous analysis is difficult.) The boundary of the wet region is then the line along which $\theta_s = \theta_c$, and within this region the precipitation is, from (4.3),

$$P = \hat{q}w = \hat{q}(\theta_s - \theta_c)/(1 - \hat{q}). \tag{8.1}$$

In this way the problem of finding the precipitation is reduced to finding the single value θ_c.
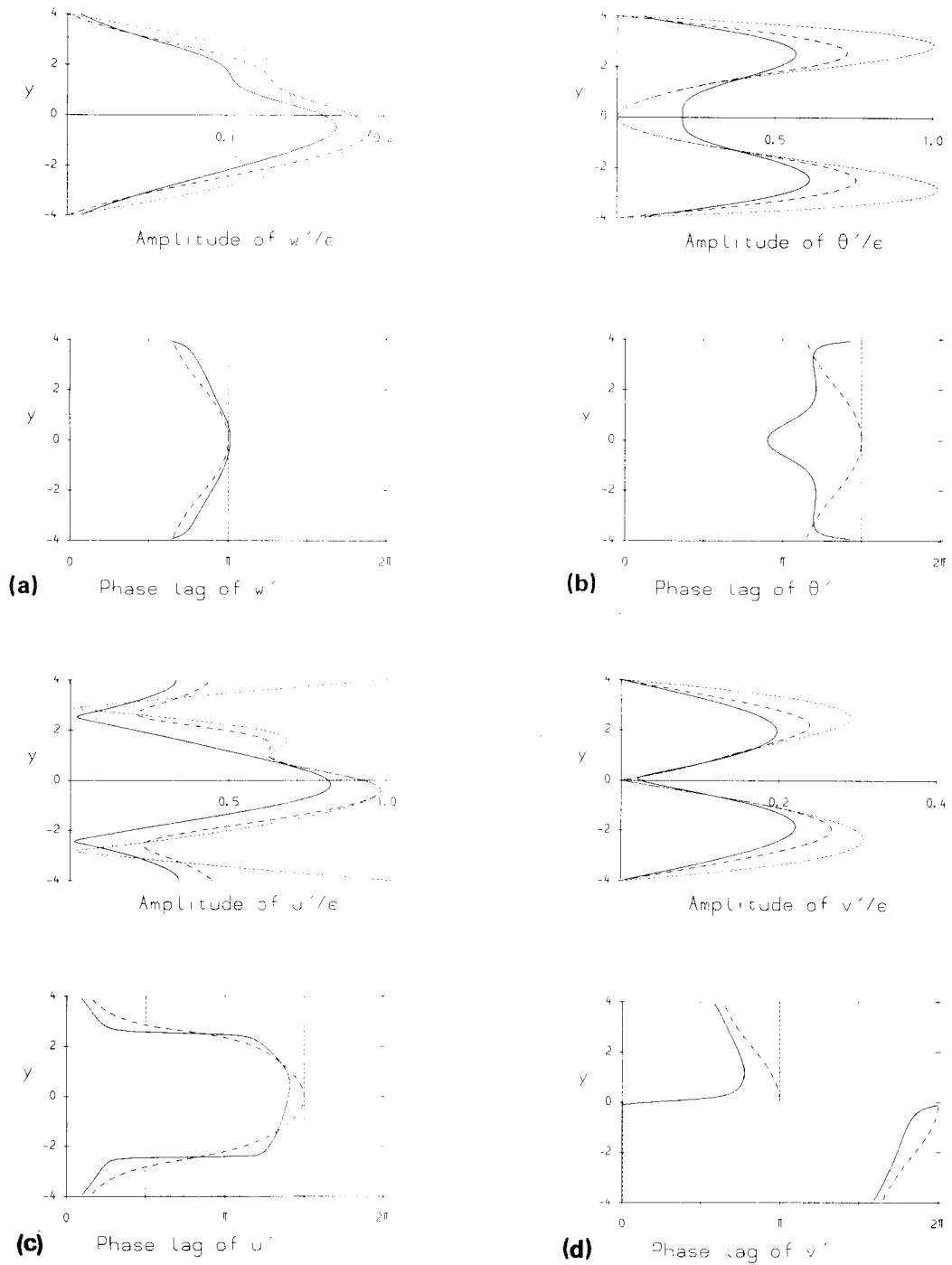
Figure 13.   The zonally varying components of the steady response to the 'January Pacific' forcing shown in Fig. 2(a), with no latent heating. Results are shown for the analytic no-friction/no-cooling (short dash curves) and no-friction models (long dash curves), together with numerical results with friction and cooling (solid curves). (a) Amplitude and phase of the mid-level vertical velocity w'/ε. This is equal to θ'_s for the no-friction/ no-cooling case. (b) Amplitude and phase of the mid-level temperature perturbation θ'/ε. (c) Amplitude and phase of the zonal low-level velocity u'/ε. (d) Amplitude and phase of the meridional low-level velocity v'/ε.

As described at the end of section 4 it is useful to regard the moist model as the superposition of two linear dry models with forcing temperatures θ_s and $\theta_L = P/\varepsilon$. Within the wet region we require $\theta = \theta_c$ and a convenient condition to determine θ_c from the dry solutions is

$$\theta_c = \theta(x_o, y_o) \text{ [due to } \theta_s] + \theta(x_o, y_o) \text{ [due to } \theta_L]. \tag{8.2}$$

(The position (x_o, y_o) is always inside the wet region.)

The problem is further simplified by neglecting contributions to θ from the zonally varying components, which are $O(\varepsilon)$ as in section 7, to reduce (8.2) to

$$\theta_c = \overline{\theta}(y_o) \text{ [due to } \overline{\theta}_s] + \overline{\theta}(y_o) \text{ [due to } \overline{\theta}_L]. \tag{8.3}$$

Precipitation estimates using a point source for θ_L in the limit $\hat{q} \to 1$ and an elliptical wet region for small $1 - \hat{q}$ are described in appendix C. As a particular example we consider the January Pacific forcing as defined in section 3, which has a maximum of 1 on the equator in the western Pacific. From the dry model we obtain

$$\overline{\theta}(y_o) \text{ [due to } \overline{\theta}_s] = 0 \cdot 7.$$

(The zonally varying contribution was $\theta'(y_o) = 0 \cdot 02$ so its omission is justified.) Evaluating the point source estimate, Eq. (C4), for total precipitation gives

$$P_{TOT} = 20\varepsilon \tag{8.4}$$

valid for $\hat{q} \to 1$. The elliptical source estimate is Eq. (C9) with θ_c determined using (8.3). Estimates of P_{TOT} and wet region area are shown in Fig. 14 for $\varepsilon = 0 \cdot 1$ and varying $\hat{q}$, along with numerical results obtained by integrating the time-dependent equations to equilibrium. Agreement is reasonable for P_{TOT}: the values differ most near $\hat{q} = 1$ where the numerical finite-difference model has difficulty resolving small wet regions. The area values diverge as area increases for decreasing $\hat{q}$, because the ellipticity assumption breaks down. The estimate (8.4) can be regarded as an easily calculated upper bound for net precipitation.

9. THE EFFECT OF VARYING THE ZONAL FORCING GRADIENT

When forcing is zonally symmetric there is a zonal band of precipitation fed by meridional low-level inflow, as in Hadley circulation. In this section we examine the effect of increasing the zonal variation in the forcing θ_s, to see at what point the zonal band of precipitation breaks and Walker-type circulation becomes evident.

Forcing of the form

$$\theta_s = \theta_W(y)[1 - \gamma \sin(\pi x/8)] \tag{9.1}$$

is used, with θ_W as defined in (3.2) for the west Pacific, for January (maximum on the equator) and July (maximum north of the equator). This choice is not meant to represent any actual physical situation, but merely to provide convenient examples. The parameter γ controls the zonal contrast in θ_s. In each case the time-dependent equations were integrated to a near-steady state at time $t = 60$ (as in section 3), using $\varepsilon = 0 \cdot 1$, $\nu = 0$, $\hat{q} = 8/9$.

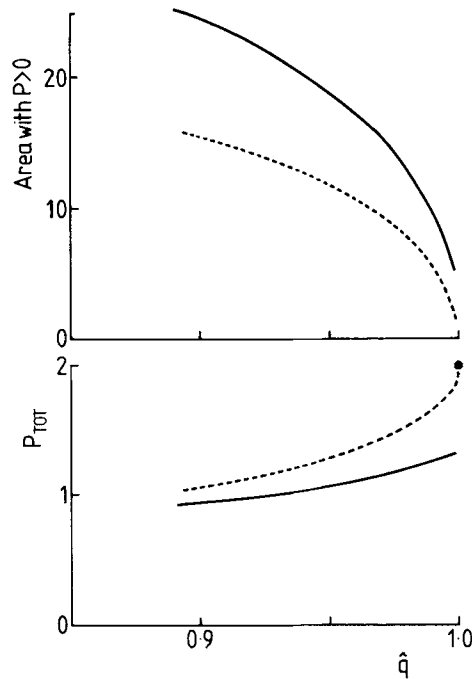This section ends with a brief description of a related seasonal cycle experiment.

Figure 14. Total precipitation P_{TOT} and area of precipitation for models with $\varepsilon = 0.1$ and various $\hat{q}$, and 'January Pacific' forcing. Solid lines are for numerical results from time-dependent integrations. The dashed lines are for estimates obtained using an elliptical precipitation region of finite width: P_{TOT} approaches a limiting value (solid circle) as $\hat{q} \rightarrow 1$.

(a) Maximum forcing on equator

With γ increasing from zero in steps of 0·01, the precipitation pattern switches from a continuous band to an elongated patch on reaching $\gamma = 0.06$. Changes in the pattern up to this point and beyond are gradual: the wet region thins and the rainband breaks near $x = 4$, where θ_s is weakest along the equator, and broadens near $x = -4$ where θ_s is strongest.

The forcing θ_s for $\gamma = 0.06$ is shown in Fig. 15, together with low-level wind components and the precipitation map. The mid-level vertical velocity pattern (not shown) is almost identical to the precipitation—low-level divergence at the equator first appears where and when the rainband breaks. Meridional low-level flow is everywhere equatorward, so any equatorial divergence must be associated with the zonal flow. Figure 15(b) shows equatorial westerlies within the precipitation region and easterlies elsewhere, reflecting a balance of frictional and pressure gradient terms along the equator. The zonal flow also contributes significantly to the convergence in the precipitation region. The temperature field (not shown) looks like the forcing pattern in Fig. 15(a), but with markedly less zonal contrast.

(b) Maximum forcing off the equator

In this case θ_s is largest at $y = 1.5$, about 15°N. When γ is again increased in steps of 0·01 there is a gradual change in the precipitation pattern, with the zonal band breaking at $\gamma = 0.20$.

Maps of θ_s, u, v and P for $\gamma = 0.20$ are shown in Fig. 16. As before, the rainband breaks near $x = 4$ where θ_s is relatively low. The map of meridional velocity shows quite
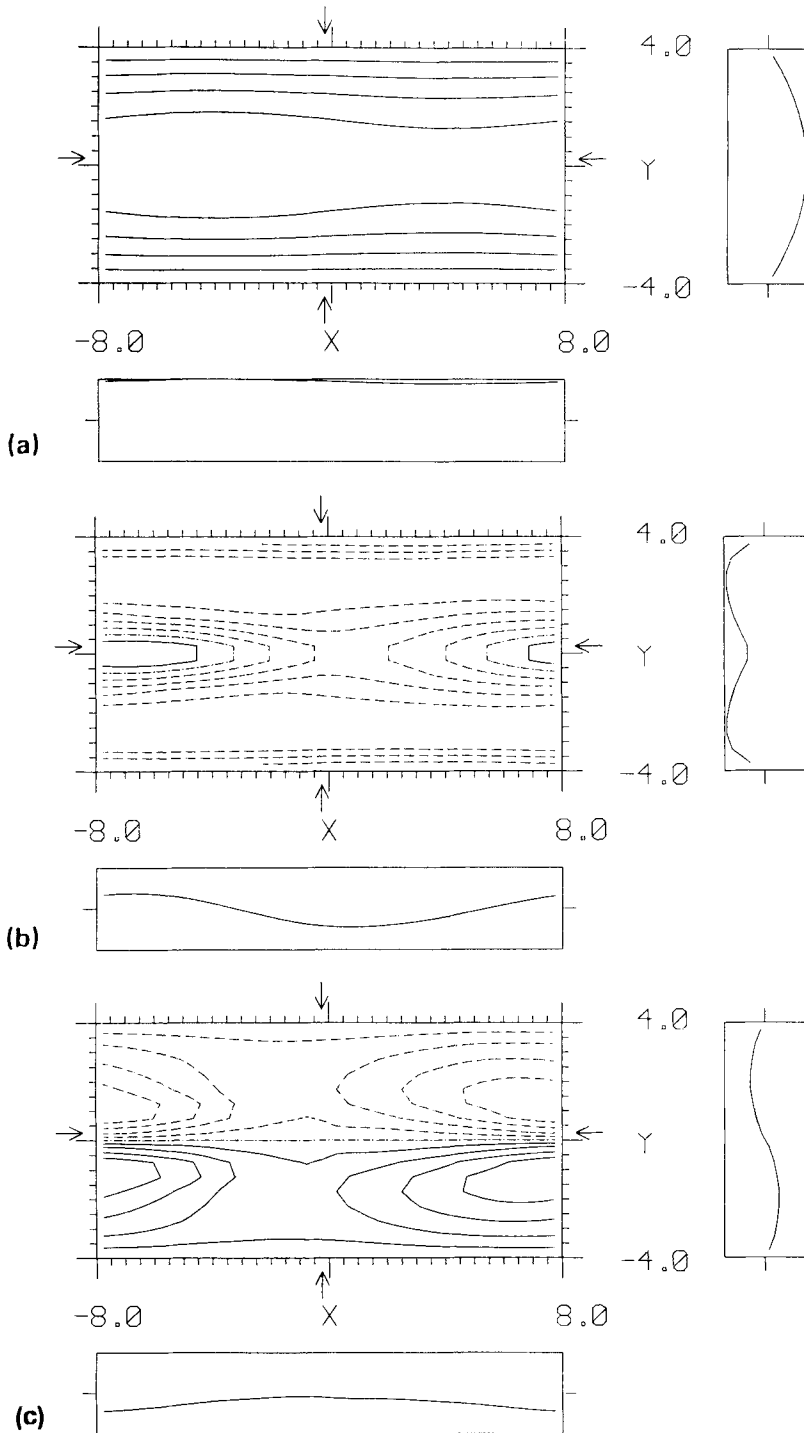
Figure 15. The response to the forcing $\theta_s = \theta_w(y)[1 - \gamma \sin(\pi x/8)]$ with $\theta_w = 1 - (y/4)^2$ and $\gamma = 0.06$, using $\varepsilon = 0.1$, $\hat{q} = 8/9$. (a) The forcing temperature θ_s with min $= 0.11$, max $= 1.1$, c.i. $=$ max/5. (b) The low-level zonal velocity u at time $t = 60$ (effectively steady) with min $= -0.24$, max $= 0.09$, c.i. $=$ min/5. The zero contour is dash-dotted, and positive contours solid. (c) The low-level meridional velocity v at time $t = 60$, with min $= -0.38$, max $= 0.38$, c.i. $=$ max/5. (d) Precipitation P at time $t = 60$ with max $= 0.06$, c.i. $=$ max/5.
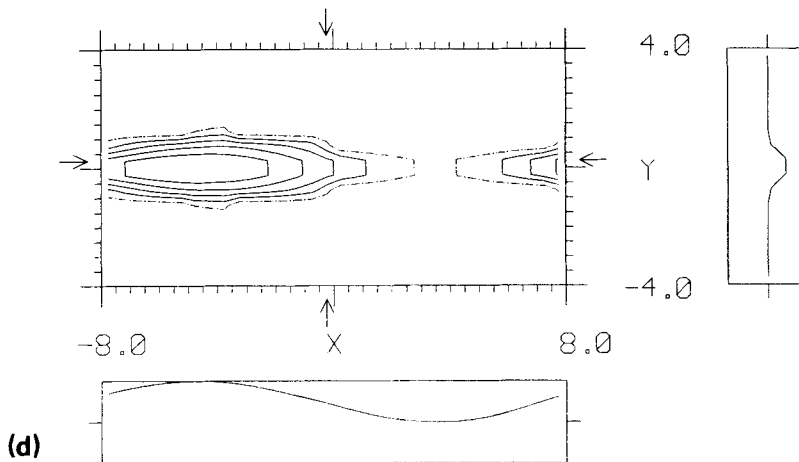
(d)

Figure 15. (Continued)

strong cross-equatorial flow directed northward into and across the region of precipitation, with weaker southward flow to the north-west of the precipitation. This component again is weakly convergent at the break in the rainband.

The zonal flow is westerly in a strip north of the equator, with maximum strength just to the west of the heaviest precipitation and minimum west of the break in the rainband. The zonal gradient is sufficient to provide the low-level divergence required at the break, and to boost convergence across the centre of the precipitation region. Just west of the break there is a 'doldrums' region of very light winds.

Compared with the previous case we see that considerably larger zonal contrast in θ_s is required to break the rainband off the equator. Due to Coriolis effects the zonal temperature gradient is less efficient at driving a zonal wind gradient away from the equator.

(c) A seasonal cycle experiment

A simple seasonal cycle experiment was carried out by prescribing

$$2\theta_s = \theta_{JAN}[1 + \cos(\omega t)] + \theta_{JUL}[1 - \cos(\omega t)] \tag{9.2}$$

where θ_{JAN} and θ_{JUL} are the January and July forcing fields described in section 3, $\omega = 2\pi/1440$ corresponds to a dimensional period of about 360 days. The maximum zonal forcing gradient changes in amplitude and location with time, being largest and closest to the equator in the model January when $t = 0$. The changes are slow compared with the atmospheric equilibration time of about 15 days (for $\varepsilon = 0.1$), and the response is found to be almost in equilibrium with θ_s at all times following an initial spin-up period. Accordingly the precipitation pattern gradually changes between those shown in Fig. 3 for January and July.

The equatorial zonal forcing contrast in January is 0·33, which is much larger than that found to break the rainband in section 9(a), so there is then a patch of precipitation located over the maximum in θ_s, with accompanying Walker-type circulation. Likewise, the July forcing zonal contrast of 0·13 north of the equator is too weak to break the rainband and a zonal precipitation pattern appears. Intermediate patterns for March and
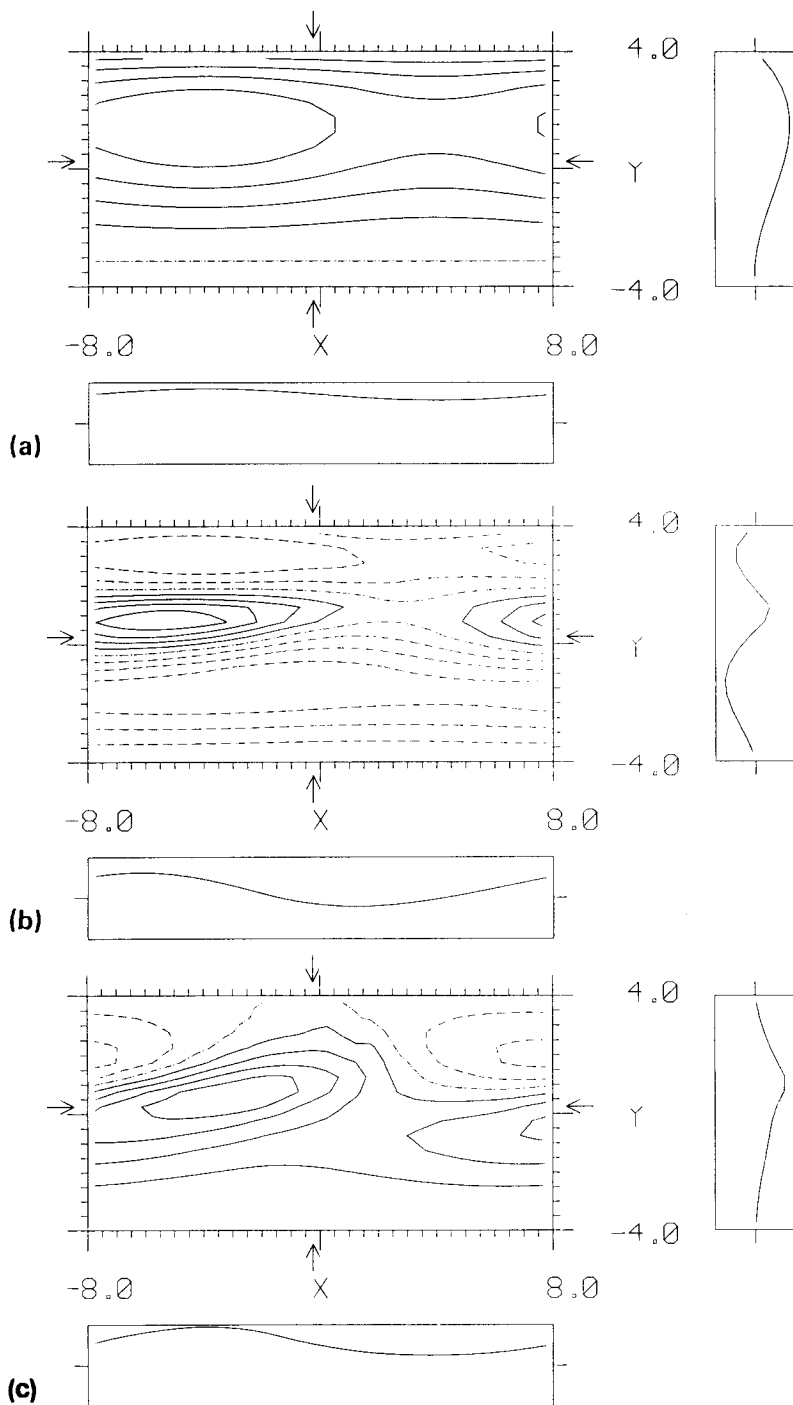
Figure 16.   The response to forcing $\theta_s = \theta_w(y)[1 - \gamma \sin(\pi x/8)]$ with

$$\theta_w = 1 - (y - Y)^2(Y^2 + 2yY + 16)/(Y^2 + 16)^2,$$

$Y = 1 \cdot 5$, and $\gamma = 0 \cdot 2$ using $\varepsilon = 0 \cdot 1$, $\hat{q} = 8/9$. (a) The forcing temperature θ_s with min $= -0 \cdot 025$, max $= 1 \cdot 2$, c.i. $= $ max/5. (b) The low-level zonal velocity u at time $t = 60$ with min $= -0 \cdot 39$, max $= 0 \cdot 5$. (c) The meridional low-level velocity v at time $t = 60$ with min $= -0 \cdot 07$, max $= 0 \cdot 14$. (d) Precipitation P at time $t = 60$ with max $= 0 \cdot 14$. c.i. $= $ max/5.

(d)

Figure 16. (Continued)

(a)

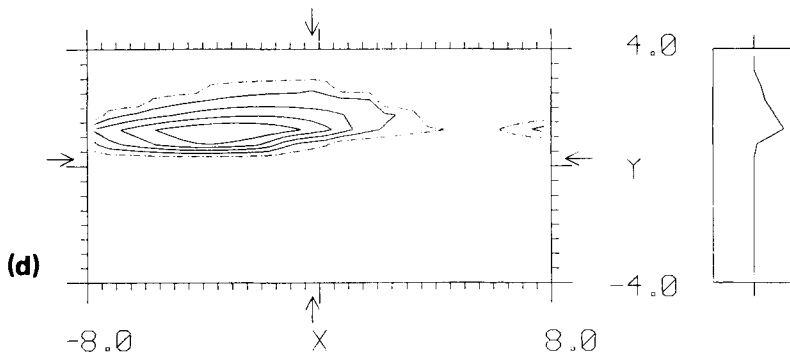**(b)**
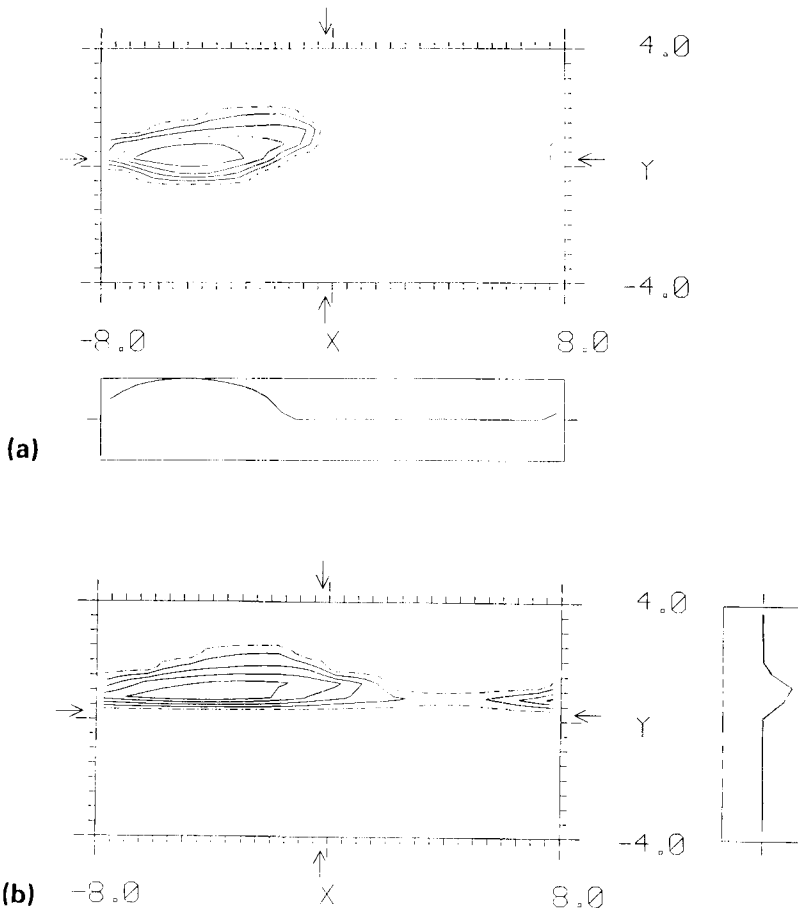
Figure 17. Precipitation patterns obtained using the seasonal cycle forcing

$$\theta_s = \tfrac{1}{2}\theta_{JAN}[1 + \cos(\pi t/720)] + \tfrac{1}{2}\theta_{JUL}[1 - \cos(\pi t/720)]$$

with $\varepsilon = 0\cdot1$, $\hat{q} = 8/9$.

(a) Time $t = 240$ (March), max $= 0\cdot10$; (b) time $t = 480$ (May), max $= 0\cdot10$. c.i. $=$ max/5.

May can be seen in Fig. 17: after January the precipitation zone shifts north of the equator, developing a north-eastward extension which then elongates to form a zonal strip. The sequence reverses from July to January.

10. CONCLUSION

A simple model with dynamic moisture effects has been used to examine the response of the tropical atmosphere to various simple heating distributions. Forcing related to sea surface temperature is prescribed, but precipitation is determined by the interaction of the atmospheric circulation and the moisture field, so the model selects its own latent heat release pattern. In the steady model, precipitation always occurs at the location of the maximum prescribed heating: at such a point low-level flow is convergent and moisture levels are soon driven to saturation both by evaporation and by low-level advection. The consequent latent heat release then adds to the prescribed heating, initiating a 'convergence feedback' process. This process is limited by the influx of surrounding drier air and by friction and Newtonian cooling.

With forcing based on idealized Pacific s.s.t., qualitatively correct precipitation patterns were obtained. In January, when s.s.t. is largest in the equatorial west Pacific, rainfall is concentrated in a patch overlying the s.s.t. maximum, whereas a continuous zonal band of rain appears in July when there is less zonal s.s.t. contrast and the maximum s.s.t. is north of the equator. For the January case circulation is Walker-like with zonal flow feeding the upward motion in the precipitation region, but in July the circulation is Hadley-like with meridional flow feeding the upward motion.

The zonally symmetric version of the model with and without latent heating is sufficiently simple to allow analytic solution of some special cases. In particular, the effect of the saturation moisture level $\hat{q}$ on the amount and extent of precipitation was analysed. The area of rainfall is closely proportional to $(1 - \hat{q})^{1/3}$, so as $\hat{q}$ approaches the critical value of 1 from below (so moist static stability changes from stable to neutral) the precipitation band shrinks toward a point above the s.s.t. maximum, while upward motion increases correspondingly. (The limit is not reached in practice, as diffusive and nonlinear effects become important on small scales.)

When zonal variations are included the problem is complicated by the two-dimensional boundary of the precipitation region, which must be determined. We estimate that the rainfall area is proportional to $(1 - \hat{q})^{1/2}$ for an elliptical pattern, and net precipitation is weakly dependent on $\hat{q}$, in general agreement with numerical results. Whether the precipitation pattern is zonal or a patch depends on the size and position of the maximum zonal forcing variation. On the equator weak variation is sufficient to drive a Walker circulation, whereas stronger variation is required to break a zonal rainband further from the equator.

With such a simple model one can think of a long list of alterations to improve the agreement with observations and to add to the physics. One aspect that was initially tested was to make $\hat{q}$ temperature dependent, as in Gill (1982b). This had only a small quantitative effect so for simplicity $\hat{q}$ was subsequently taken to be constant. Another effect tested was to allow evaporation to depend on wind speed: again the effect was small. The discontinuous nature of the precipitation-dependent static stability used here could be altered to a continuous form by allowing some precipitation to occur before saturation, and partitioning increasing q between P and q_t.

The model wind is purely baroclinic: a fixed barotropic component could be added, and one effect to be studied would be the flow required to shift precipitation away from the position of maximum prescribed heating. The simple vertical structure also means

that a proper understanding of the relation between the prescribed heating and s.s.t. is beyond the scope of this model, but this is certainly needed. Further investigations of this aspect using general circulation models of the atmosphere could be made.

The effects of land distribution have been omitted. Any model covering the entire tropics will need some representation of the continents: some preliminary calculations have been made by simply setting evaporation to zero over 'land'.

Finally, to address the problem of tropical ocean–atmosphere interaction the under-lying s.s.t. should respond in some way to atmospheric winds. A correspondingly simple ocean model is being constructed for this purpose.

APPENDIX A: STEADY ZONALLY SYMMETRIC DRY SOLUTIONS

(a) Parabolic forcing $\theta_s = 1 - (y/b)^2$
    A particular solution of (5.5) with $v \to 0$ as $|y| \to \infty$ is

$$v = -(8\varepsilon/b^2)\,\psi(y). \tag{A1}$$

Here

$$\psi(y) = \frac{cy}{2}\sum_{n=0}^{\infty} A_n(y^4/4)^n - \frac{y^3}{4}\sum_{n=0}^{\infty} B_n(y^4/4)^n \tag{A2}$$

with

$$A_0 = 1, \quad A_n = A_{n-1}/(4n+1)4n$$
$$B_0 = 1/6, \quad B_n = B_{n-1}/(4n+3)(4n+2)$$
$$c = (\pi/2)^{3/2}[2\Gamma(5/4)]^{-2} \approx 0\cdot59907.$$

This function ψ is well known in oceanography as the solution for a 'Yoshida jet', which is illustrated in Fig. 11.14 of Gill (1982a). Mathematically, $\psi/y^{1/2}$ is a Lommel function of order $1/4$ and argument $y^2/4$.

If we impose the condition $v = 0$ at the channel walls at $y = \pm b$ then free solutions of (5.5) must be added. It is convenient to use the odd and even free solutions (Abra-mowitz and Stegun 1970, section 19)

$$V_0(y) = y\sum_{n=0}^{\infty} A_n(y^4/4)^n \tag{A3a}$$

$$V_e(y) = \sum_{n=0}^{\infty} C_n(y^4/4)^n \tag{A3b}$$

with A_n as above, and

$$C_0 = 1, \quad C_n = C_{n-1}/4n(4n-1).$$

Then the solution with v vanishing on the channel walls is

$$v = -\varepsilon F(y) \tag{A4}$$

where

$$F(y) = (8/b^2)[\psi(y) - V_0(y)\psi(b)/V_0(b)]. \tag{A5}$$

(b) Point source $\theta_s = \delta(y - y_0)$

The solution to (5.5) with $v = 0$ at $y = b$ is

$$v = \begin{cases} -\varepsilon H_y(-y_o) H(y)/W & y_o < y \leqslant b \\ \varepsilon H_y(y_o) H(-y)/W & -b \leqslant y < y_o \end{cases} \qquad (A6)$$

where

$$H(y) = V_e(y) - V_o(y)V_e(b)/V_o(b) \qquad (A7)$$

and

$$W = H_y(y_o)H(-y_o) + H(y_o)H_y(-y_o) = -2V_e(b)/V_o(b)$$

is a Wronskian whose value is independent of y_o. The potential temperature is

$$\theta = \begin{cases} -H_y(-y_o)H_y(y)/W & y_o \leqslant y \leqslant b \\ -H_y(y_o)H_y(-y)/W & -b \leqslant y \leqslant y_o \end{cases} \qquad (A8)$$

and vertical velocity is simply

$$w = -\varepsilon\theta \qquad \text{for } y \neq y_o. \qquad (A9)$$

APPENDIX B: APPROXIMATE SOLUTIONS FOR THE ZONALLY SYMMETRIC MOIST MODEL

The parabolic forcing $\theta_s = 1 - (y/b)^2$ is considered. Suppose the northern edge of the wet region is at y_+: then the dry equation (5.5) can be solved in the region $y_+ \leqslant y \leqslant b$ with

$$v(b) = 0 \qquad (B1a)$$

$$v_y(y_+) = 0 \qquad (B1b)$$

to obtain

$$v = -\varepsilon[F(y) - H(y)F_y(y_+)/H_y(y_+)] \qquad (B2)$$

where $F(y)$ and $H(y)$ are as defined in appendix A. The value $v_+(y_+)$ is plotted in Fig. 12 as a function of y_+.

(a) Point source

Suppose the wet region is infinitely thin, so $y_+ \to 0$. Then the expression (B2) is simply a linear superposition of the solutions in appendix A for the dry equations forced by parabolic θ_s and by a point source. The precipitation provides an extra heating term as described at the end of section 4, with in this case known position and with magnitude determined by requiring $\theta = \theta_s$ at $y = 0$.

Equation (6.5) for P_{TOT} with $\hat{q} \to 1$ leads to the precipitation estimate

$$P_{TOT} = -2\varepsilon F_y(0)/H_y(0). \qquad (B3)$$

(b) Wet region of finite width

In the wet region centred on $y = 0$ we approximate (6.1) by

$$(1 - \hat{q})v_{yy} = -\varepsilon\theta_{sy}. \qquad (B4)$$

(This is valid for small $1 - \hat{q}$.) Integrating twice for parabolic θ_s and using symmetry and (B1b) leads to

$$(1 - \hat{q})v = \varepsilon y(y^2 - 3y_+^2)/3b^2 \tag{B5}$$

for $-y_+ \leqslant y \leqslant y_+$.

Matching (B2) and (B5) at y_+ gives an equation to solve for y_+. Then v_+ is known and P_{TOT} is given by (6.5).

For small y we can evaluate (B2) at $y = 0$ and substitute in (B5) to obtain the explicit expression

$$y_+^3 = -3b^2(1 - \hat{q})F_y(0)/2H_y(0). \tag{B6}$$

APPENDIX C: PRECIPITATION ESTIMATES

The zonal average of the forcing temperature $\theta_L = P/\varepsilon$ is

$$\overline{\theta}_L(y) = \frac{1}{l} \int_0^l \theta_L \, dx$$

where l is the length of the channel. The total precipitation is related to $\overline{\theta}_L$ by

$$P_{TOT} = \int_0^l \int_{-b}^b P \, dx \, dy = \varepsilon l \int_{-b}^b \overline{\theta}_L \, dy. \tag{C1}$$

(a) Point source

In the limit $\hat{q} \to 1$ we take the wet region to be a point source of latent heat located at (x_o, y_o) and put

$$\overline{\theta}_L = I\delta(y - y_o) \tag{C2}$$

where

$$I = P_{TOT}/\varepsilon l.$$

From appendix A,

$$\overline{\theta}(y_o) \,[\text{due to } \overline{\theta}_L] = -IH_y(-y_o)H_y(y_o)/W. \tag{C3}$$

For a point source we must have $\theta_c = \theta_s(x_o, y_o)$ so the matching condition (8.3) leads to

$$P_{TOT} = \frac{-\varepsilon l W}{H_y(-y_o)H_y(y_o)} \{\theta_s(x_o, y_o) - \overline{\theta}(y_o) \,[\text{due to } \overline{\theta}_s]\} \tag{C4}$$

where the term { } can be calculated using the linear zonally symmetric dry model.

(b) Distributed source

To extend this estimate to small $(1 - \hat{q})$, suppose that near (x_o, y_o) the prescribed forcing has the form

$$\theta_s = \theta_s(x_o, y_o) - A^2(x - x_o)^2 - B^2(y - y_o)^2. \tag{C5}$$

Then the wet region where $\theta_s \geqslant \theta_c$ is elliptical in shape. Using (8.1) we obtain in the wet region

$$\theta_L = [r^2 - A^2(x - x_o)^2 - B^2(y - y_o)^2]\hat{q}/(1 - \hat{q}) \tag{C6}$$

where

$$r^2 = \theta_s(x_0, y_0) - \theta_c. \tag{C7}$$

Hence

$$\overline{\theta}_L(y) = \begin{cases} \dfrac{4\hat{q}}{3l(1 - \hat{q})A}[r^2 - B^2(y - y_0)^2]^{3/2} & y_- < y < y_+ \\ 0 & \text{otherwise} \end{cases} \tag{C8}$$

where

$$y_+ = y_0 + r/B$$

$$y_- = y_0 - r/B.$$

(We have assumed that the elliptical wet region closes within the periodic channel.) From (C1) the net precipitation over the area $\pi r^2/AB$ of the wet region is

$$P_{\text{TOT}} = \frac{\varepsilon \pi \hat{q} r^4}{2(1 - \hat{q})AB}. \tag{C9}$$

As $\hat{q} \to 1$ the estimates (C9) and (C4) must agree, so r must be $O[(1 - \hat{q})^{1/4}]$.

The dry zonally symmetric equations can be solved with forcing $\overline{\theta}_L$ to obtain $\overline{\theta}(y_0)$ [due to $\overline{\theta}_L$] as a function of θ_c. Then θ_c, and hence r, is determined by applying the matching condition (8.3).

REFERENCES

Abramowitz, M. and Stegun, I. A.	1970	*Handbook of mathematical functions.* Dover Publications, N.Y.
Davey, M. K.	1985	Results from a moist equatorial atmosphere model. Pp. 41–49 in *Coupled ocean–atmosphere models.* (Ed. J. C. J. Nihoul). Elsevier Oceanography Series **40**
Gill, A. E.	1980	Some simple solutions for heat-induced tropical circulation. *Q. J. R. Meteorol. Soc.*, **106**, 447–462
	1982a	*Atmosphere–ocean dynamics.* Academic Press, New York, N.Y.
	1982b	Studies of moisture effects in simple atmospheric models: the stable case. *Geophys. Astrophys. Fluid Dyn.*, **19**, 119–152
	1982c	Spontaneously growing hurricane-like disturbances in a simple baroclinic model with latent heat release. Pp. 111–129 in *Topics in atmospheric and oceanic sciences: Intense atmospheric vortices.* (Ed. Bengtsson/Lighthill). Springer Verlag
	1985	Elements of coupled ocean–atmosphere models for the tropics. Pp. 303–327 in *Coupled ocean–atmosphere models* (Ed. J. C. J. Nihoul). Elsevier Oceanography Series **40**
Gill, A. E. and Phlips, P. J.	1986	Nonlinear effects on heat-induced circulations of the tropical atmosphere. *Q. J. R. Meteorol. Soc.*, **112**, 69–92
Heckley, W. A. and Gill, A. E.	1984	Some simple analytic solutions to the problem of forced equatorial long waves. *ibid.*, **110**, 203–217
Held, I. M. and Suarez, M. J.	1978	A two-level primitive equation atmospheric model designed for climatic sensitivity experiments. *J. Atmos. Sci.*, **35**, 206–229
Hirst, A. C.	1986	Unstable and damped equatorial modes in simple coupled ocean-atmosphere models. *ibid.*, **43**, 606–630
Lau, K. M. and Lim, H.	1982	Thermally driven motions in an equatorial beta-plane: Hadley and Walker circulations during the winter monsoon. *Mon. Weather Rev.*, **110**, 336–353

Lim, H. and Chang, C.-P.   1983   Dynamics of teleconnections and Walker circulations forced by equatorial heating. *J. Atmos. Sci.*, **40**, 1897–1915

Lorenz, E. N.   1984   Formulation of a low order model of a moist general circulation. *ibid.*, **41**, 1933–1945

Phlips, P. J. and Gill, A. E.   1987   An analytic model of the heat-induced tropical circulation in the presence of a mean wind. *Q. J. R. Meteorol. Soc.*, **113**, 213–236

Rowntree, P. R.   1972   The influence of tropical east Pacific Ocean temperatures on the atmosphere. *ibid.*, **98**, 290–321

Weare, B. C.   1986a   A simple model of the tropical atmosphere driven by a circulation-dependent forcing. *ibid.*, **112**, 409–429

                                 1986b   A simple model of the tropical atmosphere with circulation-dependent heating and specific humidity. *J. Atmos. Sci.*, **43**, 2001–2016

Webster, P. J.   1972   Response of the tropical atmosphere to local steady forcing. *Mon. Weather Rev.*, **100**, 518–541

                                 1981   Mechanisms determining the atmospheric response to sea surface temperature anomalies. *J. Atmos. Sci.*, **38**, 554–571

Zebiak, S. E.   1982   A simple atmospheric model of relevance to El Niño. *ibid.*, **39**, 2017–2027